

Luminosities and energies of e^+e^- collision data taken between $\sqrt{s}=4.61$ GeV and 4.95 GeV at BESIII*

M. Ablikim(麦迪娜)¹, M. N. Achasov^{11,b}, P. Adlarson⁷⁰, M. Albrecht⁴, R. Aliberti³¹, A. Amoroso^{69A,69C}, M. R. An(安美儒)³⁵, Q. An(安琪)^{53,66}, X. H. Bai(白旭红)⁶¹, Y. Bai(白羽)⁵², O. Bakina³², R. Baldini Ferroli^{26A}, I. Balossino^{27A,1}, Y. Ban(班勇)^{42,g}, V. Batozskaya^{1,40}, D. Becker³¹, K. Begzsuren²⁹, N. Berger³¹, M. Bertani^{26A}, D. Bettoni^{27A}, F. Bianchi^{69A,69C}, J. Bloms⁶³, A. Bortone^{69A,69C}, I. Boyko³², R. A. Briere⁵, A. Brueggemann⁶³, H. Cai(蔡浩)⁷¹, X. Cai(蔡啸)^{1,53}, A. Calcaterra^{26A}, G. F. Cao(曹国富)^{1,58}, N. Cao(曹宁)^{1,58}, S. A. Cetin^{57A}, J. F. Chang(常劲帆)^{1,53}, W. L. Chang(常万玲)^{1,58}, G. Chelkov^{32,a}, C. Chen(陈琛)³⁹, Chao Chen(陈超)⁵⁰, G. Chen(陈刚)¹, H. S. Chen(陈和生)^{1,58}, M. L. Chen(陈玛丽)^{1,53}, S. J. Chen(陈申见)³⁸, S. M. Chen(陈少敏)⁵⁶, T. Chen¹, X. R. Chen(陈旭荣)^{28,58}, X. T. Chen¹, Y. B. Chen(陈元柏)^{1,53}, Z. J. Chen(陈卓俊)^{23,h}, W. S. Cheng(成伟帅)^{69C}, X. Chu(初晓)³⁹, G. Cibinetto^{27A}, F. Cossio^{69C}, J. J. Cui(崔佳佳)⁴⁵, H. L. Dai(代洪亮)^{1,53}, J. P. Dai(代建平)⁷³, A. Dbeyssi¹⁷, R. E. de Boer⁴, D. Dedovich³², Z. Y. Deng(邓子艳)¹, A. Denig³¹, I. Denysenko³², M. Destefanis^{69A,69C}, F. De Mori^{69A,69C}, Y. Ding(丁勇)³⁶, J. Dong(董静)^{1,53}, L. Y. Dong(董燎原)^{1,58}, M. Y. Dong(董明义)¹, X. Dong(董翔)⁷¹, S. X. Du(杜书先)⁷⁵, P. Egorov^{32,a}, Y. L. Fan(范玉兰)⁷¹, J. Fang(方建)^{1,53}, S. S. Fang(房双世)^{1,58}, W. X. Fang(方文兴)¹, Y. Fang(方易)¹, R. Farinelli^{27A}, L. Fava^{69B,69C}, F. Feldbauer⁴, G. Felici^{26A}, C. Q. Feng(封常青)^{53,66}, J. H. Feng(冯俊华)⁵⁴, K. Fischer⁶⁴, M. Fritsch⁴, C. Fritsch⁶³, C. D. Fu(傅成栋)¹, H. Gao(高涵)⁵⁸, Y. N. Gao(高原宁)^{42,g}, Yang Gao(高扬)^{53,66}, S. Garbolino^{69C}, I. Garzia^{27A,27B}, P. T. Ge(葛潘婷)⁷¹, Z. W. Ge(葛振武)³⁸, C. Geng(耿聪)⁵⁴, E. M. Gersabeck⁶², A. Gilman⁶⁴, K. Goetzen¹², L. Gong(龚丽)³⁶, W. X. Gong(龚文煊)^{1,53}, W. Grad³¹, M. Greco^{69A,69C}, L. M. Gu(谷立民)³⁸, M. H. Gu(顾昱皓)^{1,53}, Y. T. Gu(顾运斤)¹⁴, C. Y. Guan(关春懿)^{1,58}, A. Q. Guo(郭爱强)^{28,58}, L. B. Guo(郭立波)³⁷, R. P. Guo(郭如盼)⁴⁴, Y. P. Guo(郭玉萍)^{10,f}, A. Guskov^{32,a}, T. T. Han(韩婷婷)⁴⁵, W. Y. Han(韩文颖)³⁵, X. Q. Hao(郝喜庆)¹⁸, F. A. Harris⁶⁰, K. K. He(何凯凯)⁵⁰, K. L. He(何康林)^{1,58}, F. H. Heinsius⁴, C. H. Heinz³¹, Y. K. Heng(衡月昆)¹, C. Herold⁵⁵, M. Himmelreich^{12,d}, G. Y. Hou(侯国一)^{1,58}, Y. R. Hou(侯颖锐)⁵⁸, Z. L. Hou(侯治龙)¹, H. M. Hu(胡海明)^{1,58}, J. F. Hu^{51,i}, T. Hu(胡涛)¹, Y. Hu(胡誉)¹, G. S. Huang(黄光顺)^{53,66}, K. X. Huang(黄凯旋)⁵⁴, L. Q. Huang(黄麟钦)⁶⁷, L. Q. Huang(黄麟钦)^{28,58}, X. T. Huang(黄性涛)⁴⁵, Y. P. Huang(黄燕萍)¹, Z. Huang(黄震)^{42,g}, T. Hussain⁶⁸, N. Hüsen^{25,31}, W. Imoehl²⁵, M. Irshad^{53,66}, J. Jackson²⁵, S. Jaeger⁴, S. Janchiv²⁹, Q. Ji(纪全)¹, Q. P. Ji(姬清平)¹⁸, X. B. Ji(季晓斌)^{1,58}, X. L. Ji(季筱璐)^{1,53}, Y. Y. Ji(吉钰瑶)⁴⁵, Z. K. Jia(贾泽坤)^{53,66}, H. B. Jiang(姜侯兵)⁴⁵, S. S. Jiang(姜赛赛)³⁵, X. S. Jiang(江晓山)¹, Y. Jiang⁵⁸, J. B. Jiao(焦健斌)⁴⁵, Z. Jiao(焦铮)²¹, S. Jin(金山)³⁸, Y. Jin(金毅)⁶¹, M. Q. Jing(荆茂强)^{1,58}, T. Johansson⁷⁰, N. Kalantar-Nayestanaki⁵⁹, X. S. Kang(康晓珅)³⁶, R. Kappert⁵⁹, B. C. Ke(柯百谦)⁷⁵, I. K. Keshk⁴, A. Khokuz⁶³, P. Kiese³¹, R. Kiuchi¹, R. Kliemt¹², L. Koch³³, O. B. Kolcu^{57A}, B. Kopf⁴, M. Kuemmel⁴, M. Kuessner⁴, A. Kupsc^{40,70}, W. Kühn³³, J. J. Lane⁶², J. S. Lange³³, P. Larin¹⁷, A. Lavania²⁴, L. Lavezzi^{69A,69C}, Z. H. Lei(雷祥弘)^{53,66}, H. Leithoff³¹, M. Lellmann³¹, T. Lenz³¹, C. Li(李翠)⁴³, C. Li(李聪)³⁹, C. H. Li(李春花)³⁵, Cheng Li(李澄)^{53,66}, D. M. Li(李德民)⁷⁵, F. Li(李飞)^{1,53}, G. Li(李刚)¹, H. Li(李慧)⁴⁷, H. Li(李贺)^{53,66}, H. B. Li(李海波)^{1,58}, H. J. Li(李惠静)¹⁸, H. N. Li^{51,i}, J. Q. Li⁴, J. S. Li(李静舒)⁵⁴, J. W. Li(李井文)⁴⁵, Ke Li(李科)¹, L. J. Li(李林健)¹, L. K. Li(李龙科)¹, Lei Li(李蕾)³, M. H. Li(李明浩)³⁹, P. R. Li(李培荣)^{34,j,k}, S. X. Li(李素娴)¹⁰, S. Y. Li(栗帅迎)⁵⁶, T. Li(李腾)⁴⁵, W. D. Li(李卫东)^{1,58}, W. G. Li(李卫国)¹, X. H. Li(李旭红)^{53,66}, X. L. Li(李晓玲)⁴⁵, Xiaoyu Li(李

Received xxxx June xxxx

* Supported in part by National Key R&D Program of China under Contracts Nos. 2020YFA0406400, 2020YFA0406300; National Natural Science Foundation of China (NSFC) under Contracts Nos. 11635010, 11735014, 11805086, 11835012, 11935015, 11935016, 11935018, 11961141012, 12022510, 12025502, 12035009, 12035013, 12192260, 12192261, 12192262, 12192263, 12192264, 12192265; the Chinese Academy of Sciences (CAS) Large-Scale Scientific Facility Program; Joint Large-Scale Scientific Facility Funds of the NSFC and CAS under Contract No. U1832207; CAS Key Research Program of Frontier Sciences under Contract No. QYZDJ-SSW-SLH040; 100 Talents Program of CAS; Fundamental Research Funds for the Central Universities, Lanzhou University, University of Chinese Academy of Sciences; The Institute of Nuclear and Particle Physics (INPAC) and Shanghai Key Laboratory for Particle Physics and Cosmology; ERC under Contract No. 758462; European Union's Horizon 2020 research and innovation programme under Marie Skłodowska-Curie grant agreement under Contract No. 894790; German Research Foundation DFG under Contracts Nos. 443159800, Collaborative Research Center CRC 1044, GRK 2149; Istituto Nazionale di Fisica Nucleare, Italy; Ministry of Development of Turkey under Contract No. DPT2006K-120470; National Science and Technology fund; National Science Research and Innovation Fund (NSRF) via the Program Management Unit for Human Resources & Institutional Development, Research and Innovation under Contract No. B16F640076; STFC (United Kingdom); Suranaree University of Technology (SUT), Thailand Science Research and Innovation (TSRI), and National Science Research and Innovation Fund (NSRF) under Contract No. 160355; The Royal Society, UK under Contracts Nos. DH140054, DH160214; The Swedish Research Council; U. S. Department of Energy under Contract No. DE-FG02-05ER41374.

晓宇)^{1,58}, H. Liang(梁昊)^{53,66}, H. Liang(梁浩)^{1,58}, H. Liang(梁浩)³⁰, Y. F. Liang(梁勇飞)⁴⁹, Y. T. Liang(梁羽铁)^{28,58}, G. R. Liao(廖广睿)¹³, L. Z. Liao(廖龙洲)⁴⁵, J. Libby²⁴, A. Limphirat⁵⁵, C. X. Lin(林创新)⁵⁴, D. X. Lin(林德旭)^{28,58}, T. Lin¹, B. J. Liu(刘北江)¹, C. X. Liu(刘春秀)¹, D. Liu^{17,66}, F. H. Liu(刘福虎)⁴⁸, Fang Liu(刘芳)¹, Feng Liu(刘峰)⁶, G. M. Liu^{51,i}, H. Liu^{34,j,k}, H. B. Liu(刘宏邦)¹⁴, H. M. Liu(刘怀民)^{1,58}, Huanhuan Liu(刘欢欢)¹, Huihui Liu(刘汇慧)¹⁹, J. B. Liu(刘建北)^{53,66}, J. L. Liu(刘佳俊)⁶⁷, J. Y. Liu(刘晶译)^{1,58}, K. Liu(刘凯)¹, K. Y. Liu(刘魁勇)³⁶, Ke Liu(刘珂)²⁰, L. Liu(刘亮)^{53,66}, Lu Liu(刘露)³⁹, M. H. Liu(刘美宏)^{10,f}, P. L. Liu(刘佩莲)¹, Q. Liu(刘倩)⁵⁸, S. B. Liu(刘树彬)^{53,66}, T. Liu(刘桐)^{10,f}, W. K. Liu(刘维克)³⁹, W. M. Liu(刘卫民)^{53,66}, X. Liu(刘翔)^{34,j,k}, Y. Liu(刘英)^{34,j,k}, Y. B. Liu(刘玉斌)³⁹, Z. A. Liu(刘振安)¹, Z. Q. Liu(刘智青)⁴⁵, X. C. Lou(娄辛丑)¹, F. X. Lu(卢飞翔)⁵⁴, H. J. Lu(吕海江)²¹, J. G. Lu(吕军光)^{1,53}, X. L. Lu(陆小玲)¹, Y. Lu(卢宇)⁷, Y. P. Lu(卢云鹏)^{1,53}, Z. H. Lu¹, C. L. Luo(罗成林)³⁷, M. X. Luo(罗民兴)⁷⁴, T. Luo(罗涛)^{10,f}, X. L. Luo(罗小兰)^{1,53}, X. R. Lyu(吕晓睿)⁵⁸, Y. F. Lyu(吕翌丰)³⁹, F. C. Ma(马凤才)³⁶, H. L. Ma(马海龙)¹, L. L. Ma(马连良)⁴⁵, M. M. Ma(马明明)^{1,58}, Q. M. Ma(马秋梅)¹, R. Q. Ma(马润秋)^{1,58}, R. T. Ma(马瑞廷)⁵⁸, X. Y. Ma(马晓妍)^{1,53}, Y. Ma(马尧)^{42,g}, F. E. Maas¹⁷, M. Maggiora^{69A,69C}, S. Maldaner⁴, S. Malde⁶⁴, Q. A. Malik⁶⁸, A. Mangoni^{26B}, Y. J. Mao(冒亚军)^{42,g}, Z. P. Mao(毛泽普)¹, S. Marcello^{69A,69C}, Z. X. Meng(孟召霞)⁶¹, J. G. Messchendorp⁵⁹, G. Mezzadri^{27A,1}, H. Miao¹, T. J. Min(闵天觉)³⁸, R. E. Mitchell²⁵, X. H. Mo(莫晓虎)¹, N. Yu. Muchnoi^{11,b}, Y. Nefedov³², F. Nerling^{17,d}, I. B. Nikolaev^{11,b}, Z. Ning(宁哲)^{1,53}, S. Nisar^{9,l}, Y. Niu(牛艳)⁴⁵, S. L. Olsen⁵⁸, Q. Ouyang(欧阳群)¹, S. Pacetti^{26B,26C}, X. Pan(潘祥)^{10,f}, Y. Pan(潘越)⁵², A. Pathak³⁰, M. Pelizaesus⁴, H. P. Peng(彭海平)^{53,66}, K. Peters^{12,d}, J. L. Ping(平加伦)³⁷, R. G. Ping(平荣刚)^{1,58}, S. Plura³¹, S. Pogodin³², V. Prasad^{53,66}, F. Z. Qi(齐法制)¹, H. Qi(齐航)^{53,66}, H. R. Qi(漆红荣)⁵⁶, M. Qi(祁鸣)³⁸, T. Y. Qi(齐天钰)^{10,f}, S. Qian(钱森)^{1,53}, W. B. Qian(钱文斌)⁵⁸, Z. Qian(钱圳)⁵⁴, C. F. Qiao(乔从丰)⁵⁸, J. J. Qin(秦佳佳)⁶⁷, L. Q. Qin(秦丽清)¹³, X. P. Qin(覃潇平)^{10,f}, X. S. Qin(秦小帅)⁴⁵, Z. H. Qin(秦中华)^{1,53}, J. F. Qiu(邱进发)¹, S. Q. Qu(屈三强)⁵⁶, K. H. Rashid⁶⁸, C. F. Redmer³¹, K. J. Ren(任旷浩)³⁵, A. Rivetti^{69C}, V. Rodin⁵⁹, M. Rolo^{69C}, G. Rong(荣刚)^{1,58}, Ch. Rosner¹⁷, S. N. Ruan(阮氏宁)³⁹, H. S. Sang(桑昊榆)⁶⁶, A. Sarantsev^{32,c}, Y. Schelhaas³¹, C. Schmier⁴, K. Schoenning⁷⁰, M. Scodreggio^{27A,27B}, K. Y. Shan(尚科羽)^{10,f}, W. Shan(单葳)²², X. Y. Shan(单心钰)^{53,66}, J. F. Shanguan(上官剑锋)⁵⁰, L. G. Shao(邵立港)^{1,58}, M. Shao(邵明)^{53,66}, C. P. Shen(沈成平)^{10,f}, H. F. Shen(沈宏飞)^{1,58}, X. Y. Shen(沈肖雁)^{1,58}, B. A. Shi(施伯安)⁵⁸, H. C. Shi(石煌超)^{53,66}, J. Y. Shi(石京燕)¹, q. q. Shi(石勤强)⁵⁰, R. S. Shi(师荣盛)^{1,58}, X. Shi(史欣)^{1,53}, X. D. Shi(师晓东)^{53,66}, J. J. Song(宋娇娇)¹⁸, W. M. Song(宋维民)^{1,30}, Y. X. Song(宋昀轩)^{42,g}, S. Sosio^{69A,69C}, S. Spataro^{69A,69C}, F. Stieler³¹, K. X. Su(苏可馨)⁷¹, P. P. Su(苏彭彭)⁵⁰, Y. J. Su(粟杨捷)⁵⁸, G. X. Sun(孙功星)¹, H. Sun⁵⁸, H. K. Sun(孙浩凯)¹, J. F. Sun(孙俊峰)¹⁸, L. Sun(孙亮)⁷¹, S. S. Sun(孙胜森)^{1,58}, T. Sun(孙童)^{1,58}, W. Y. Sun(孙文玉)³⁰, X. Sun(孙翔)^{23,h}, Y. J. Sun(孙勇杰)^{53,66}, Y. Z. Sun(孙永昭)¹, Z. T. Sun(孙振田)⁴⁵, Y. H. Tan(谭英华)⁷¹, Y. X. Tan(谭雅星)^{53,66}, C. J. Tang(唐昌建)⁴⁹, G. Y. Tang(唐光毅)¹, J. Tang(唐健)⁵⁴, L. Y. Tao(陶璐燕)⁶⁷, Q. T. Tao(陶秋田)^{23,h}, M. Tat⁶⁴, J. X. Teng(滕佳秀)^{53,66}, V. Thoren⁷⁰, W. H. Tian(田文辉)⁴⁷, Y. Tian(田野)^{28,58}, I. Uman^{57B}, B. Wang(王斌)¹, B. L. Wang(王滨龙)⁵⁸, C. W. Wang(王成伟)³⁸, D. Y. Wang(王大勇)^{42,g}, F. Wang(王菲)⁶⁷, H. J. Wang(王泓鉴)^{34,j,k}, H. P. Wang(王宏鹏)^{1,58}, K. Wang(王科)^{1,53}, L. L. Wang(王亮亮)¹, M. Wang(王萌)⁴⁵, M. Z. Wang(王梦真)^{42,g}, Meng Wang(王蒙)^{1,58}, S. Wang¹³, S. Wang(王顺)^{10,f}, T. Wang(王婷)^{10,f}, T. J. Wang(王腾蛟)³⁹, W. Wang(王为)⁵⁴, W. H. Wang(王文欢)⁷¹, W. P. Wang(王维平)^{53,66}, X. Wang(王轩)^{42,g}, X. F. Wang(王雄飞)^{34,j,k}, X. L. Wang(王小龙)^{10,f}, Y. Wang(王亦)⁵⁶, Y. D. Wang(王雅迪)⁴¹, Y. F. Wang(王贻芳)¹, Y. H. Wang(王英豪)⁴³, Y. Q. Wang(王雨晴)¹, Yaqian Wang(王亚乾)^{1,16}, Z. Wang(王铮)^{1,53}, Z. Y. Wang(王至勇)^{1,58}, Ziyi Wang(王子一)⁵⁸, D. H. Wei(魏代会)¹³, F. Weidner⁶³, S. P. Wen(文硕频)¹, D. J. White⁶², U. Wiedner⁴, G. Wilkinson⁶⁴, M. Wolke⁷⁰, L. Wollenberg⁴, J. F. Wu(吴金飞)^{1,58}, L. H. Wu(伍灵慧)¹, L. J. Wu(吴连近)^{1,58}, X. Wu(吴潇)^{10,f}, X. H. Wu(伍雄浩)³⁰, Y. Wu⁶⁶, Z. Wu(吴智)^{1,53}, L. Xia(夏磊)^{53,66}, T. Xiang(相腾)^{42,g}, D. Xiao(肖栋)^{34,j,k}, G. Y. Xiao(肖光延)³⁸, H. Xiao(肖浩)^{10,f}, S. Y. Xiao(肖素玉)¹, Y. L. Xiao(肖云龙)^{10,f}, Z. J. Xiao(肖振军)³⁷, C. Xie(谢陈)³⁸, X. H. Xie(谢昕海)^{42,g}, Y. Xie(谢勇)⁴⁵, Y. G. Xie(谢宇广)^{1,53}, Y. H. Xie(谢跃红)⁶, Z. P. Xie(谢智鹏)^{53,66}, T. Y. Xing(邢天宇)^{1,58}, C. F. Xu¹, C. J. Xu(许创杰)⁵⁴, G. F. Xu(许国发)¹, H. Y. Xu(许皓月)⁶¹, Q. J. Xu(徐庆君)¹⁵, X. P. Xu(徐新平)⁵⁰, Y. C. Xu(胥英超)^{58,76}, Z. P. Xu(许泽鹏)³⁸, F. Yan(严芳)^{10,f}, L. Yan(严亮)^{10,f}, W. B. Yan(鄢文标)^{53,66}, W. C. Yan(闫文成)⁷⁵, H. J. Yang(杨海军)^{46,e}, H. L. Yang(杨昊霖)³⁰, H. X. Yang(杨洪勋)¹, L. Yang(杨玲)⁴⁷, S. L. Yang⁵⁸, Tao Yang(杨涛)¹, Y. F. Yang(杨艳芳)³⁹, Y. X. Yang(杨逸翔)^{1,58}, Yifan Yang(杨翊凡)^{1,58}, M. Ye(叶梅)^{1,53}, M. H. Ye(叶铭汉)⁸, J. H. Yin(殷俊昊)¹, Z. Y. You(尤郑昀)⁵⁴, B. X. Yu(俞伯祥)¹, C. X. Yu(喻纯旭)³⁹, G. Yu(余刚)^{1,58}, T. Yu(于涛)⁶⁷, C. Z. Yuan(苑长征)^{1,58}, L. Yuan(袁丽)², S. C. Yuan¹, X. Q. Yuan(袁晓庆)¹, Y. Yuan(袁野)^{1,58}, Z. Y. Yuan(袁朝阳)⁵⁴, C. X. Yue(岳崇兴)³⁵, A. A. Zafar⁶⁸, F. R. Zeng(曾凡蕊)⁴⁵, X. Zeng(曾鑫)⁶, Y. Zeng(曾云)^{23,h}, Y. H. Zhan(詹永华)⁵⁴, A. Q. Zhang(张安庆)¹, B. L. Zhang¹, B. X. Zhang(张丙新)¹, D. H. Zhang(张丹昊)³⁹, G. Y. Zhang(张广义)¹⁸, H. Zhang⁶⁶, H. H. Zhang(张宏浩)⁵⁴, H. H. Zhang(张宏宏)³⁰, H. Y. Zhang(章红宇)^{1,53}, J. L. Zhang(张杰磊)⁷², J. Q. Zhang(张敬庆)³⁷, J. W. Zhang(张家文)¹, J. X. Zhang^{34,j,k}, J. Y. Zhang(张建勇)¹, J. Z. Zhang(张景芝)^{1,58}, Jianyu Zhang(张剑宇)^{1,58}, Jiawei Zhang(张嘉伟)^{1,58}, L. M. Zhang(张黎明)⁵⁶, L. Q. Zhang(张丽青)⁵⁴, Lei Zhang(张雷)³⁸, P. Zhang¹, Q. Y. Zhang(张秋岩)^{35,75}, Shuihan Zhang(张水涵)^{1,58}, Shulei Zhang(张书磊)^{23,h}, X. D. Zhang(张小东)⁴¹, X. M. Zhang¹, X. Y. Zhang(张学尧)⁴⁵, X. Y. Zhang(张旭颜)⁵⁰, Y. Zhang⁶⁴, Y. T. Zhang(张亚腾)⁷⁵, Y. H. Zhang(张银鸿)^{1,53}, Yan Zhang(张言)^{53,66}, Yao Zhang(张瑶)¹, Z. H. Zhang¹, Z. Y. Zhang(张振宇)⁷¹, Z. Y. Zhang(张子羽)³⁹, G. Zhao(赵光)¹, J. Zhao(赵静)³⁵,

J. Y. Zhao(赵静宜)^{1,58}, J. Z. Zhao(赵京周)^{1,53}, Lei Zhao(赵雷)^{53,66}, Ling Zhao(赵玲)¹, M. G. Zhao(赵明刚)³⁹, Q. Zhao(赵强)¹, S. J. Zhao(赵书俊)⁷⁵, Y. B. Zhao(赵豫斌)^{1,53}, Y. X. Zhao(赵宇翔)^{28,58}, Z. G. Zhao(赵政国)^{53,66}, A. Zhemchugov^{32,a}, B. Zheng(郑波)⁶⁷, J. P. Zheng(郑建平)^{1,53}, Y. H. Zheng(郑阳恒)⁵⁸, B. Zhong(钟彬)³⁷, C. Zhong(钟翠)⁶⁷, X. Zhong(钟鑫)⁵⁴, H. Zhou(周航)⁴⁵, L. P. Zhou(周利鹏)^{1,58}, X. Zhou(周详)⁷¹, X. K. Zhou(周晓康)⁵⁸, X. R. Zhou(周小蓉)^{53,66}, X. Y. Zhou(周兴玉)³⁵, Y. Z. Zhou(周卓)^{10,f}, J. Zhu(朱江)³⁹, K. Zhu(朱凯)¹, K. J. Zhu(朱科军)¹, L. X. Zhu(朱琳莹)⁵⁸, S. H. Zhu(朱世海)⁶⁵, S. Q. Zhu(朱仕强)³⁸, T. J. Zhu(朱腾蛟)⁷², W. J. Zhu(朱文静)^{10,f}, Y. C. Zhu(朱莹春)^{53,66}, Z. A. Zhu(朱自安)^{1,58}, B. S. Zou(邹冰松)¹, J. H. Zou(邹佳恒)¹

(BESIII Collaboration)

¹ *Institute of High Energy Physics, Beijing 100049, People's Republic of China*

² *Beihang University, Beijing 100191, People's Republic of China*

³ *Beijing Institute of Petrochemical Technology, Beijing 102617, People's Republic of China*

⁴ *Bochum Ruhr-University, D-44780 Bochum, Germany*

⁵ *Carnegie Mellon University, Pittsburgh, Pennsylvania 15213, USA*

⁶ *Central China Normal University, Wuhan 430079, People's Republic of China*

⁷ *Central South University, Changsha 410083, People's Republic of China*

⁸ *China Center of Advanced Science and Technology, Beijing 100190, People's Republic of China*

⁹ *COMSATS University Islamabad, Lahore Campus, Defence Road, Off Raiwind Road, 54000 Lahore, Pakistan*

¹⁰ *Fudan University, Shanghai 200433, People's Republic of China*

¹¹ *G.I. Budker Institute of Nuclear Physics SB RAS (BINP), Novosibirsk 630090, Russia*

¹² *GSI Helmholtzcentre for Heavy Ion Research GmbH, D-64291 Darmstadt, Germany*

¹³ *Guangxi Normal University, Guilin 541004, People's Republic of China*

¹⁴ *Guangxi University, Nanning 530004, People's Republic of China*

¹⁵ *Hangzhou Normal University, Hangzhou 310036, People's Republic of China*

¹⁶ *Hebei University, Baoding 071002, People's Republic of China*

¹⁷ *Helmholtz Institute Mainz, Staudinger Weg 18, D-55099 Mainz, Germany*

¹⁸ *Henan Normal University, Xinxiang 453007, People's Republic of China*

¹⁹ *Henan University of Science and Technology, Luoyang 471003, People's Republic of China*

²⁰ *Henan University of Technology, Zhengzhou 450001, People's Republic of China*

²¹ *Huangshan College, Huangshan 245000, People's Republic of China*

²² *Hunan Normal University, Changsha 410081, People's Republic of China*

²³ *Hunan University, Changsha 410082, People's Republic of China*

²⁴ *Indian Institute of Technology Madras, Chennai 600036, India*

²⁵ *Indiana University, Bloomington, Indiana 47405, USA*

²⁶ (A) *INFN Laboratori Nazionali di Frascati, I-00044, Frascati, Italy*; (B) *INFN Sezione di Perugia, I-06100, Perugia, Italy*; (C) *University of Perugia, I-06100, Perugia, Italy*

²⁷ (A) *INFN Sezione di Ferrara, I-44122, Ferrara, Italy*; (B) *University of Ferrara, I-44122, Ferrara, Italy*

²⁸ *Institute of Modern Physics, Lanzhou 730000, People's Republic of China*

²⁹ *Institute of Physics and Technology, Peace Avenue 54B, Ulaanbaatar 13330, Mongolia*

³⁰ *Jilin University, Changchun 130012, People's Republic of China*

³¹ *Johannes Gutenberg University of Mainz, Johann-Joachim-Becher-Weg 45, D-55099 Mainz, Germany*

³² *Joint Institute for Nuclear Research, 141980 Dubna, Moscow region, Russia*

³³ *Justus-Liebig-Universitaet Giessen, II. Physikalisches Institut, Heinrich-Buff-Ring 16, D-35392 Giessen, Germany*

³⁴ *Lanzhou University, Lanzhou 730000, People's Republic of China*

³⁵ *Liaoning Normal University, Dalian 116029, People's Republic of China*

³⁶ *Liaoning University, Shenyang 110036, People's Republic of China*

³⁷ *Nanjing Normal University, Nanjing 210023, People's Republic of China*

³⁸ *Nanjing University, Nanjing 210093, People's Republic of China*

³⁹ *Nankai University, Tianjin 300071, People's Republic of China*

⁴⁰ *National Centre for Nuclear Research, Warsaw 02-093, Poland*

⁴¹ *North China Electric Power University, Beijing 102206, People's Republic of China*

⁴² *Peking University, Beijing 100871, People's Republic of China*

⁴³ *Qufu Normal University, Qufu 273165, People's Republic of China*

⁴⁴ *Shandong Normal University, Jinan 250014, People's Republic of China*

⁴⁵ *Shandong University, Jinan 250100, People's Republic of China*

⁴⁶ *Shanghai Jiao Tong University, Shanghai 200240, People's Republic of China*

⁴⁷ *Shanxi Normal University, Linfen 041004, People's Republic of China*

- ⁴⁸ Shanxi University, Taiyuan 030006, People's Republic of China
- ⁴⁹ Sichuan University, Chengdu 610064, People's Republic of China
- ⁵⁰ Soochow University, Suzhou 215006, People's Republic of China
- ⁵¹ South China Normal University, Guangzhou 510006, People's Republic of China
- ⁵² Southeast University, Nanjing 211100, People's Republic of China
- ⁵³ State Key Laboratory of Particle Detection and Electronics, Beijing 100049, Hefei 230026, People's Republic of China
- ⁵⁴ Sun Yat-Sen University, Guangzhou 510275, People's Republic of China
- ⁵⁵ Suranaree University of Technology, University Avenue 111, Nakhon Ratchasima 30000, Thailand
- ⁵⁶ Tsinghua University, Beijing 100084, People's Republic of China
- ⁵⁷ (A)Istinye University, 34010, Istanbul, Turkey; (B)Near East University, Nicosia, North Cyprus, Mersin 10, Turkey
- ⁵⁸ University of Chinese Academy of Sciences, Beijing 100049, People's Republic of China
- ⁵⁹ University of Groningen, NL-9747 AA Groningen, The Netherlands
- ⁶⁰ University of Hawaii, Honolulu, Hawaii 96822, USA
- ⁶¹ University of Jinan, Jinan 250022, People's Republic of China
- ⁶² University of Manchester, Oxford Road, Manchester, M13 9PL, United Kingdom
- ⁶³ University of Muenster, Wilhelm-Klemm-Strasse 9, 48149 Muenster, Germany
- ⁶⁴ University of Oxford, Keble Road, Oxford OX13RH, United Kingdom
- ⁶⁵ University of Science and Technology Liaoning, Anshan 114051, People's Republic of China
- ⁶⁶ University of Science and Technology of China, Hefei 230026, People's Republic of China
- ⁶⁷ University of South China, Hengyang 421001, People's Republic of China
- ⁶⁸ University of the Punjab, Lahore-54590, Pakistan
- ⁶⁹ (A)University of Turin, I-10125, Turin, Italy; (B)University of Eastern Piedmont, I-15121, Alessandria, Italy; (C)INFN, I-10125, Turin, Italy
- ⁷⁰ Uppsala University, Box 516, SE-75120 Uppsala, Sweden
- ⁷¹ Wuhan University, Wuhan 430072, People's Republic of China
- ⁷² Xinyang Normal University, Xinyang 464000, People's Republic of China
- ⁷³ Yunnan University, Kunming 650500, People's Republic of China
- ⁷⁴ Zhejiang University, Hangzhou 310027, People's Republic of China
- ⁷⁵ Zhengzhou University, Zhengzhou 450001, People's Republic of China
- ⁷⁶ Yantai University, Yantai 264005, People's Republic of China
- ^a Also at the Moscow Institute of Physics and Technology, Moscow 141700, Russia
- ^b Also at the Novosibirsk State University, Novosibirsk, 630090, Russia
- ^c Also at the NRC "Kurchatov Institute", PNPI, 188300, Gatchina, Russia
- ^d Also at Goethe University Frankfurt, 60323 Frankfurt am Main, Germany
- ^e Also at Key Laboratory for Particle Physics, Astrophysics and Cosmology, Ministry of Education; Shanghai Key Laboratory for Particle Physics and Cosmology; Institute of Nuclear and Particle Physics, Shanghai 200240, People's Republic of China
- ^f Also at Key Laboratory of Nuclear Physics and Ion-beam Application (MOE) and Institute of Modern Physics, Fudan University, Shanghai 200443, People's Republic of China
- ^g Also at State Key Laboratory of Nuclear Physics and Technology, Peking University, Beijing 100871, People's Republic of China
- ^h Also at School of Physics and Electronics, Hunan University, Changsha 410082, China
- ⁱ Also at Guangdong Provincial Key Laboratory of Nuclear Science, Institute of Quantum Matter, South China Normal University, Guangzhou 510006, China
- ^j Also at Frontiers Science Center for Rare Isotopes, Lanzhou University, Lanzhou 730000, People's Republic of China
- ^k Also at Lanzhou Center for Theoretical Physics, Lanzhou University, Lanzhou 730000, People's Republic of China
- ^l Also at the Department of Mathematical Sciences, IBA, Karachi, Pakistan

Abstract From December 2019 to June 2021, the BESIII experiment collected about 5.85 fb^{-1} of data at center-of-mass energies between 4.61 GeV and 4.95 GeV. This is the highest collision energy BEPCII has reached so far. The accumulated e^+e^- annihilation data samples are useful for studying charmonium(-like) states and charmed-hadron decays. By adopting a novel method of analyzing the production of $\Lambda_c^+\bar{\Lambda}_c^-$ pairs in e^+e^- annihilation, the center-of-mass energies are measured with a precision of $\sim 0.6 \text{ MeV}$. Integrated luminosities are measured with a precision of better than 1% by analyzing the events of large-angle Bhabha

scattering. These measurements provide important inputs to the analyses based on these data samples.

Key words Luminosity, Center-of-mass energy, BESIII detector

1 Introduction

In 2020, BEPCII implemented an energy upgrade project and increased the maximum center-of-mass energy from 4.61 GeV to 4.95 GeV. During the data-taking years of 2020 and 2021, the BESIII experiment collected e^+e^- annihilation data at 12 center-of-mass energy (E_{cms}) points between 4.61 GeV and 4.95 GeV. In this energy region, a few charmonium(-like) states can be produced, such as the Y(4630) and Y(4660) [1–5], which are potential candidates for multi-quark states other than the charmonium states [6]. More strikingly, at 4.68 GeV, the BESIII experiment observed the first candidate for a charged hidden-charm tetraquark with strangeness, $Z_{cs}(3985)^+$ [7]. Note that charge conjugation is always implied. In addition, the $\Lambda_c^+\bar{\Lambda}_c^-$ pair-production is open in this energy region. This provides many opportunities for precise measurements of the properties of the lightest charmed baryon Λ_c^+ , with threshold production and quantum coherence of the accumulated $\Lambda_c^+\bar{\Lambda}_c^-$ pairs. In 2014, the BESIII experiment collected 567 pb^{-1} of e^+e^- annihilation data at 4.599 GeV, which led to many pioneering measurements [8–14]. About ten times more $\Lambda_c^+\bar{\Lambda}_c^-$ pair events are expected to be contained in all data taken above 4.6 GeV, which provides great potential to improve our knowledge of the strong and weak interactions in the charm sector [15]. The E_{cms} and integrated luminosities of these data samples are important inputs for the analyses using these data samples.

In this paper, we present measurements of E_{cms} and integrated luminosities for data samples at various energy points, as listed in Table 1. The Beam Energy Measurement System (BEMS) [16], which was installed in 2008, is designed to precisely measure the beam energy based on the energies of Compton back-scattered photons. However, the working range of BEMS is below 4 GeV which implies the measurement of E_{cms} for data samples involved in this paper have to be performed offline. A novel method of using $e^+e^- \rightarrow \Lambda_c^+\bar{\Lambda}_c^-$ events is adopted, which was discussed in the energy measurement for the $\psi(3770)$ data at BESIII [17]. In the luminosity measurement, the Bhabha scattering process $e^+e^- \rightarrow (\gamma) e^+e^-$ is used, benefiting from its clear signature and large production cross section, which allow for a negligible statistical uncertainty and relatively small systematic uncertainty. A cross check of the luminosity

results is performed by analyzing the di-photon process $e^+e^- \rightarrow (\gamma) \gamma\gamma$.

2 The BESIII detector and MC simulations

The BESIII detector [18] records symmetric e^+e^- collisions provided by the BEPCII storage ring [19], which operates at center-of-mass energies ranging from 2.0 GeV to 4.95 GeV. BESIII has collected large data samples in this energy region [20]. The cylindrical core of the BESIII detector covers 93% of the full solid angle and consists of a helium-based multilayer drift chamber (MDC), a plastic scintillator time-of-flight system (TOF), and a CsI(Tl) electromagnetic calorimeter (EMC), which are all enclosed in a superconducting solenoidal magnet providing a 1.0 T magnetic field. The solenoid is supported by an octagonal flux-return yoke with resistive plate counter muon identification modules interleaved with steel. The charged-particle momentum resolution at 1 GeV/c is 0.5%, and the dE/dx resolution is 6% for electrons from Bhabha scattering. The EMC measures photon energies with a resolution of 2.5% (5%) at 1 GeV in the barrel (end cap) region. The time resolution in the TOF barrel region is 68 ps, while that in the end cap region is 60 ps [21].

Simulated samples produced with a GEANT4-based [22] Monte Carlo (MC) package, which includes the geometric description of the BESIII detector and the detector response, are used to determine detection efficiencies and to estimate backgrounds. The simulation models the beam energy spread and initial state radiation (ISR) in the e^+e^- annihilations with the generator KKMC [23]. The inclusive MC sample includes the production of the process $\Lambda_c^+\bar{\Lambda}_c^-$ using the Born cross section line shape measured by BESIII, open charm processes, the ISR production of vector charmonium(-like) states, and the continuum processes incorporated in KKMC [23]. The known decay modes are modelled with EVTGEN [24] using branching fractions taken from the Particle Data Group (PDG) [25], and the remaining unknown charmonium decays are modelled with LUNDCHARM [27]. Final state radiation (FSR) from charged final state particles is incorporated using PHOTOS [28].

3 Measurement of center-of-mass energies

In the process $e^+e^- \rightarrow \Lambda_c^+ \bar{\Lambda}_c^-$, each Λ_c^+ ($\bar{\Lambda}_c^-$) baryon carries half the energy of the E_{cms} . Hence, the E_{cms} is obtained from the calibrated beam energy E_{Λ_c} using the reconstructed mass of one Λ_c with the following equations:

$$\begin{aligned} E_{\text{cms}} &= 2E_{\Lambda_c}, \\ E_{\Lambda_c}^2 &= E_0^2 + m_{\Lambda_c}^2 c^4 - M_{\text{BC}}^2 c^4. \end{aligned} \quad (1)$$

Here, E_0 is the uncalibrated beam energy, with input values of 2306, 2313, 2320, 2330, 2340, 2350, 2370, 2375, 2390, 2420, 2457 and 2473 MeV, respectively, for the beam energies of 12 different energy points, and m_{Λ_c} is the known Λ_c mass of 2286.46 ± 0.14 MeV/ c^2 [25, 26]. The M_{BC} is the fitted peak position of the beam-constrained mass of the Λ_c baryon calculated by $M_{\text{BC}} c^2 = \sqrt{E_0^2 - p_{\Lambda_c}^2} c^2$, where p_{Λ_c} is the momentum of the Λ_c measured in the center-of-mass system of the e^+e^- collision. Essentially, Eq. (1) is equivalent to $E_{\Lambda_c}^2 = p_{\Lambda_c}^2 c^2 + m_{\Lambda_c}^2 c^4$. The distributions of M_{BC} , instead of p_{Λ_c} are fitted, since the M_{BC} has better resolution and its fit quality is more easily controlled. According to the above analysis, we expect the calibrated beam energy E_{Λ_c} to be stable when different E_0 are used and that is well verified by both real data and MC simulations.

To perform this measurement, we use the partial reconstruction method and only one Λ_c^+ is reconstructed which the $\Lambda_c^+ \rightarrow pK^-\pi^+$ channel is used because of its relatively large decay rate and low background contamination. Each charged track must satisfy the following criteria. The distance of the closest approach of every charged track to the e^+e^- interaction point (IP) is required to be within 10 cm along the beam direction and within 1 cm in the plane perpendicular to the beam direction. The polar angle θ between the direction of a charged track and that of the positron beam must satisfy $|\cos\theta| < 0.93$ for an effective measurement in the active volume of the MDC. The dE/dx information recorded by the MDC and the time-of-flight information measured by the TOF are combined to calculate particle identification (PID) probabilities for various particle hypotheses. Tracks are identified as protons if their PID probabilities (\mathcal{P}) satisfy $\mathcal{P}(p) > \mathcal{P}(K)$ and $\mathcal{P}(p) > \mathcal{P}(\pi)$, while charged kaons and pions are identified using $\mathcal{P}(K) > \mathcal{P}(\pi)$ and $\mathcal{P}(\pi) > \mathcal{P}(K)$, respectively. All $pK^-\pi^+$ combinations in one event are kept for further study. In the fit to the M_{BC} distributions, the signals are described by the Bukin function [30] and

the backgrounds are described by a linear function. The fit result of the 4680 MeV data sample is shown in Fig. 1.

In order to validate the analysis method, an input and output (I/O) check based on the inclusive MC simulation is performed. The systematic shifts (0.09 ~ 0.25 MeV) are noticed between the measured beam energies and the true simulated input values mainly due to the ISR effect. The shifts at different energy points are taken into account as individual correction factors. The final values of the determined E_{cms} are listed in Table 1.

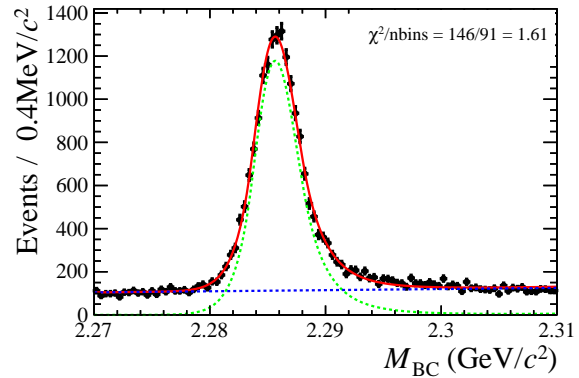


Figure 1. Fit to the M_{BC} distribution for $\Lambda_c^+ \rightarrow pK^-\pi^+$ candidates from the 4680 MeV data sample. The dotted green line is the fitted signal and the dotted blue line is the fitted background. Black dots with error bars are data, the red line is the sum of fit functions.

The systematic uncertainty for the E_{cms} measurement is mainly from the uncertainty of the Λ_c mass quoted from the PDG, which is 0.28 MeV (twice the uncertainty of the Λ_c PDG mass). Other small uncertainties are due to the M_{BC} fit range and the ISR correction. For the fit range, we vary the fit boundary and repeat the M_{BC} fit. The maximum relative changes on the E_{cms} are taken as the systematic uncertainties.

For the ISR correction, we consider the cross section line shape and the influence of the background. An alternative cross section line shape is first obtained by varying the measured Born cross section line shape of $e^+e^- \rightarrow \Lambda_c^+ \bar{\Lambda}_c^-$ process within uncertainties. The alternative and nominal line shape are used to generate signal MC samples of the process $e^+e^- \rightarrow \Lambda_c^+ \bar{\Lambda}_c^-$, where one Λ_c decays to $pK\pi$, and the other Λ_c decays inclusively, and then the I/O procedure is repeated to get the ISR correction factors. The differences in the ISR correction factors are regarded as the systematic uncertainties. In order to

take into account potential effect of background simulation, the difference in the ISR correction between the signal MC sample and the inclusive MC sample is regarded as a systematic uncertainty.

For the signal and background shapes, the uncertainties are negligible based on MC simulation studies. A summary of systematic uncertainties is given in Table 2. For each energy point, the total systematic uncertainty is taken as the quadrature sum of each item.

We validate the energy measurements to the 12 data samples using the $e^+e^- \rightarrow D^+D^{*-}$ process, where the D^+ is reconstructed via $D^+ \rightarrow K^-\pi^+\pi^+$. The recoil mass of the D^+ , RM_{D^+} , is defined as

$$RM_{D^+} = \sqrt{(E_{\text{cms}} - E_{D^+})^2/c^4 - (\vec{p}_{\text{cms}} - \vec{p}_{D^+})^2/c^2}, \quad (2)$$

where E_{D^+} (\vec{p}_{D^+}) is the energy (momentum) of the reconstructed D^+ . The total energy (momentum) of the initial e^+e^- system, E_{cms} (\vec{p}_{cms}), is input according to our measurement. The peak values of the RM_{D^+} distributions correspond to the known mass of the D^{*-} [25]. To improve the mass resolution [29], the variable $RM_{D^+} + M_{D^+} - m_{D^+}$ is adopted to represent the D^+ recoil mass spectrum, where M_{D^+} is the D^+ invariant mass, and m_{D^+} is the known D^+ mass [25]. The Bukin function is used to fit the $RM_{D^+} + M_{D^+} - m_{D^+}$ distribution to get the peak mass position, in which the tail shapes in the signal function are fixed according to MC simulation of the process $e^+e^- \rightarrow D^+D^{*-}$. Following the same procedure used for the ISR correction in the nominal analysis, the measured mass of the D^{*-} in the validation sample shows consistency with the known D^{*-} mass [25]. Figure 2 shows the mass difference at each energy point, which is consistent with zero and hence validates the measured center-of-mass energies.

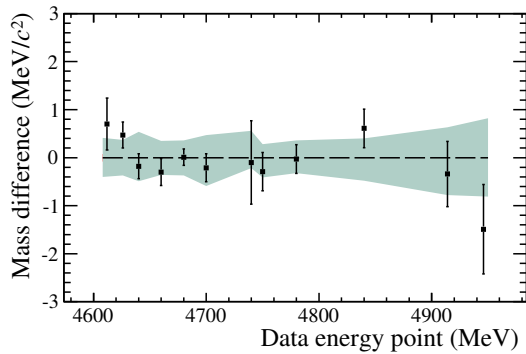


Figure 2. At each energy point, the difference between the measured D^{*-} mass using the validation sample of $e^+e^- \rightarrow D^+D^{*-}$ and the known D^{*-} mass [25]. Points with error bars

are from data and the green band is the uncertainty due to that of the E_{cms} value.

4 Measurement of integrated luminosities

The integrated luminosity of the data sample is determined by

$$\mathcal{L} = \frac{N_{e^+e^- \rightarrow X}^{\text{obs}}}{\sigma_{e^+e^- \rightarrow X}^{\text{obs}} \times \epsilon_{e^+e^- \rightarrow X}}, \quad (3)$$

where X denotes any specific final state produced in e^+e^- annihilations, $N_{e^+e^- \rightarrow X}^{\text{obs}}$ is the observed yield for the $e^+e^- \rightarrow X$ process, \mathcal{L} is the integrated luminosity for data and $\sigma_{e^+e^- \rightarrow X}^{\text{obs}}$ is the visible cross section. Here, the Bhabha process ($e^+e^- \rightarrow (\gamma)e^+e^-$) is analyzed in the nominal method, and the di-photon $e^+e^- \rightarrow (\gamma)\gamma\gamma$ process serves as a cross check channel. The observed cross sections for the two processes are provided by the BabaYaga@NLO generator [31] with 0.1% precision. The configuration parameters for the BabaYaga@NLO generator in generating Bhabha events are listed in Table 3.

The criteria used for selecting Bhabha candidates include the following. We require only two oppositely charged tracks (nCharged) detected in the MDC that satisfy $|\cos\theta| < 0.8$ and the distance requirement of the closest approach of each charged track to the IP is the same as described in Section 3. Figure 3 shows the distributions of momentum, polar angle $\cos\theta$ and azimuthal angle ϕ for the electron and positron tracks measured in the MDC in data and signal MC samples. Good consistency between data and MC simulation is shown. The momentum of each track is required to be larger than 2 GeV/c to reject backgrounds from hadronic processes. In addition, to suppress the backgrounds from di-photon process, $|\Delta\phi^{\text{EMC}}|$ is required to be in the range $[5^\circ, 40^\circ]$, where $\Delta\phi^{\text{EMC}} = |\phi_1^{\text{EMC}} - \phi_2^{\text{EMC}}| - 180^\circ$ and $\phi_{1,2}^{\text{EMC}}$ are the azimuthal angles of the two clusters produced by the electron and positron in the EMC in the center-of-mass frame.

Figure 4 shows the two-dimensional E^{EMC} distributions of e^+ and e^- of Bhabha candidate events, where E^{EMC} is the output of the deposited energies of clusters in the EMC. Due to the unexpected saturation effect [32] from a small fraction of EMC electronic readouts, E^{EMC} of the electron and positron becomes underestimated and distributes around 0.4 GeV, much less than the expected energies. As shown in Fig. 4(a), a fraction (2 ~ 9%) of the electron or positron tracks, depending on the track momentum, is influenced by the EMC saturation effect. To

Table 1. Numerical results for the center-of-mass energy E_{cms} , the integrated luminosity measured with the Bhabha process $\mathcal{L}_{\text{Bhabha}}$, the integrated luminosity measured with the di-photon process $\mathcal{L}_{\text{di-photon}}$ and their ratio for all data samples. For the E_{cms} and $\mathcal{L}_{\text{Bhabha}}$ measurements, the first uncertainty is statistical and the second is systematic. For the $\mathcal{L}_{\text{di-photon}}$ measurement, only statistical uncertainties are presented. For the ratio of $\mathcal{L}_{\text{di-photon}}$ to $\mathcal{L}_{\text{Bhabha}}$ all presented uncertainties are considered.

Sample	E_{cms} (MeV)	$\mathcal{L}_{\text{Bhabha}}$ (pb^{-1})	$\mathcal{L}_{\text{di-photon}}$ (pb^{-1})	Ratio (%)
4610	4611.86±0.12±0.30	103.65±0.05±0.55	103.37±0.13	99.73±0.59
4620	4628.00±0.06±0.32	521.53±0.11±2.76	520.17±0.28	99.74±0.55
4640	4640.91±0.06±0.38	551.65±0.12±2.92	550.67±0.29	99.82±0.55
4660	4661.24±0.06±0.29	529.43±0.12±2.81	527.53±0.29	99.64±0.55
4680	4681.92±0.08±0.29	1667.39±0.21±8.84	1665.88±0.51	99.91±0.54
4700	4698.82±0.10±0.36	535.54±0.12±2.84	533.66±0.29	99.64±0.55
4740	4739.70±0.20±0.30	163.87±0.07±0.87	165.08±0.16	100.74±0.58
4750	4750.05±0.12±0.29	366.55±0.10±1.94	367.57±0.24	100.28±0.56
4780	4780.54±0.12±0.30	511.47±0.12±2.71	512.03±0.29	100.11±0.55
4840	4843.07±0.20±0.31	525.16±0.12±2.78	526.01±0.30	100.16±0.55
4920	4918.02±0.34±0.34	207.82±0.08±1.10	208.09±0.19	100.13±0.57
4950	4950.93±0.36±0.38	159.28±0.07±0.84	159.85±0.17	100.36±0.58

Table 2. Systematic uncertainties for the E_{cms} measurement (in MeV). For each energy point, the total systematic uncertainty corresponds to the quadrature sum of each item.

Source	Sample											
	4610	4620	4640	4660	4680	4700	4740	4750	4780	4840	4920	4950
PDG mass	0.28	0.28	0.28	0.28	0.28	0.28	0.28	0.28	0.28	0.28	0.28	0.28
Fit range	0.04	0.14	0.22	0.04	0.04	0.14	0.04	0.04	0.04	0.02	0.17	0.24
ISR correction	0.10	0.06	0.13	0.07	0.06	0.17	0.11	0.04	0.09	0.13	0.09	0.08
Total	0.30	0.32	0.38	0.29	0.29	0.36	0.30	0.29	0.30	0.31	0.34	0.38

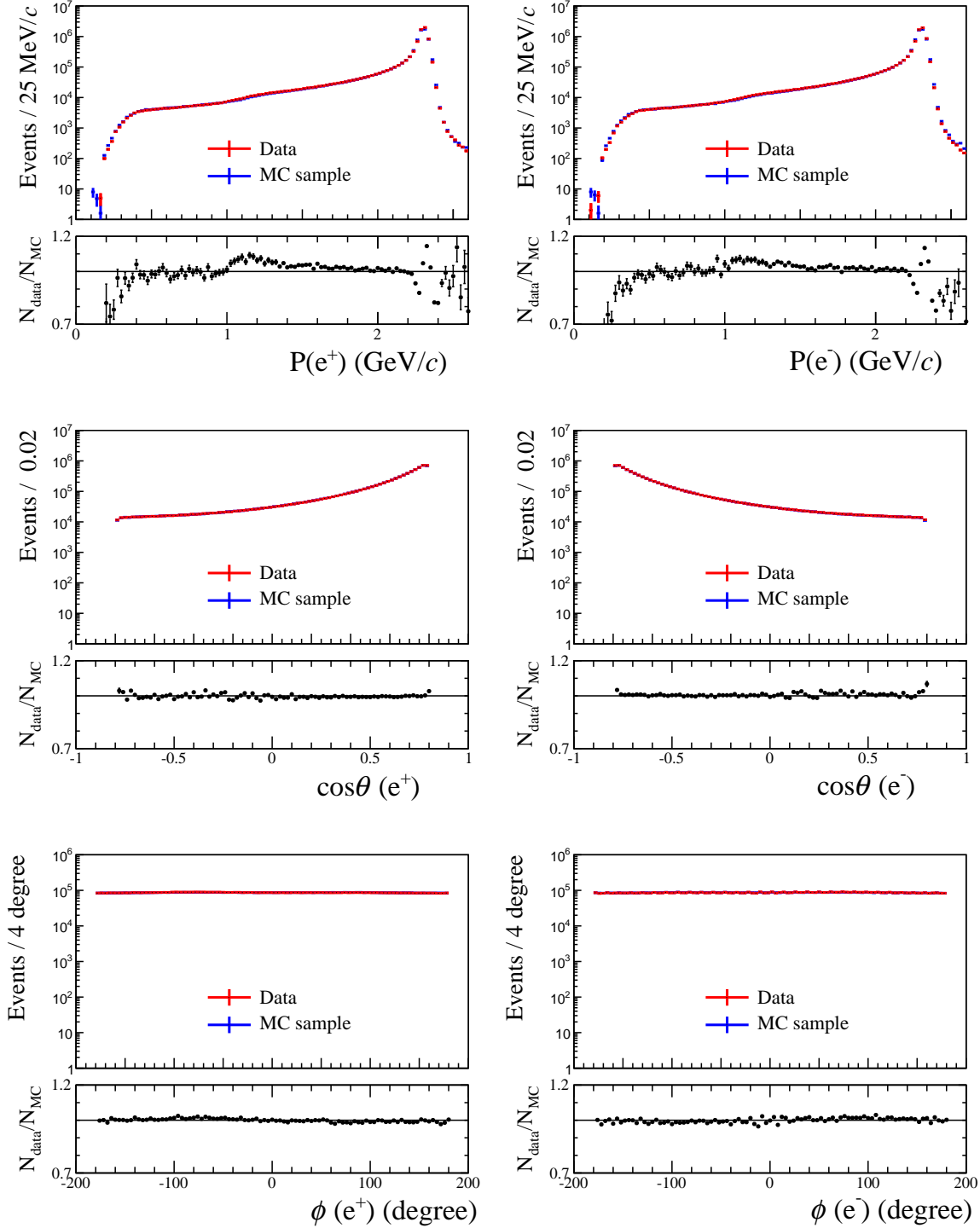


Figure 3. Comparisons between the data and MC samples at the 4620 MeV energy point for the momentum (top), $\cos\theta$ (middle) and ϕ (bottom) distributions for the e^+ (left) and e^- (right) in Bhabha events. N_{data}/N_{MC} is the ratio of the data and MC samples. Red points with error bars are data and the blue points are MC samples. The sizes of the MC samples are normalized to those in data. Except for the variable to be shown, all other requirements used in the event selection have been applied. Although comparison shows inconsistency in high momentum region of the momentum spectrum, this would not have much effect on the final results.

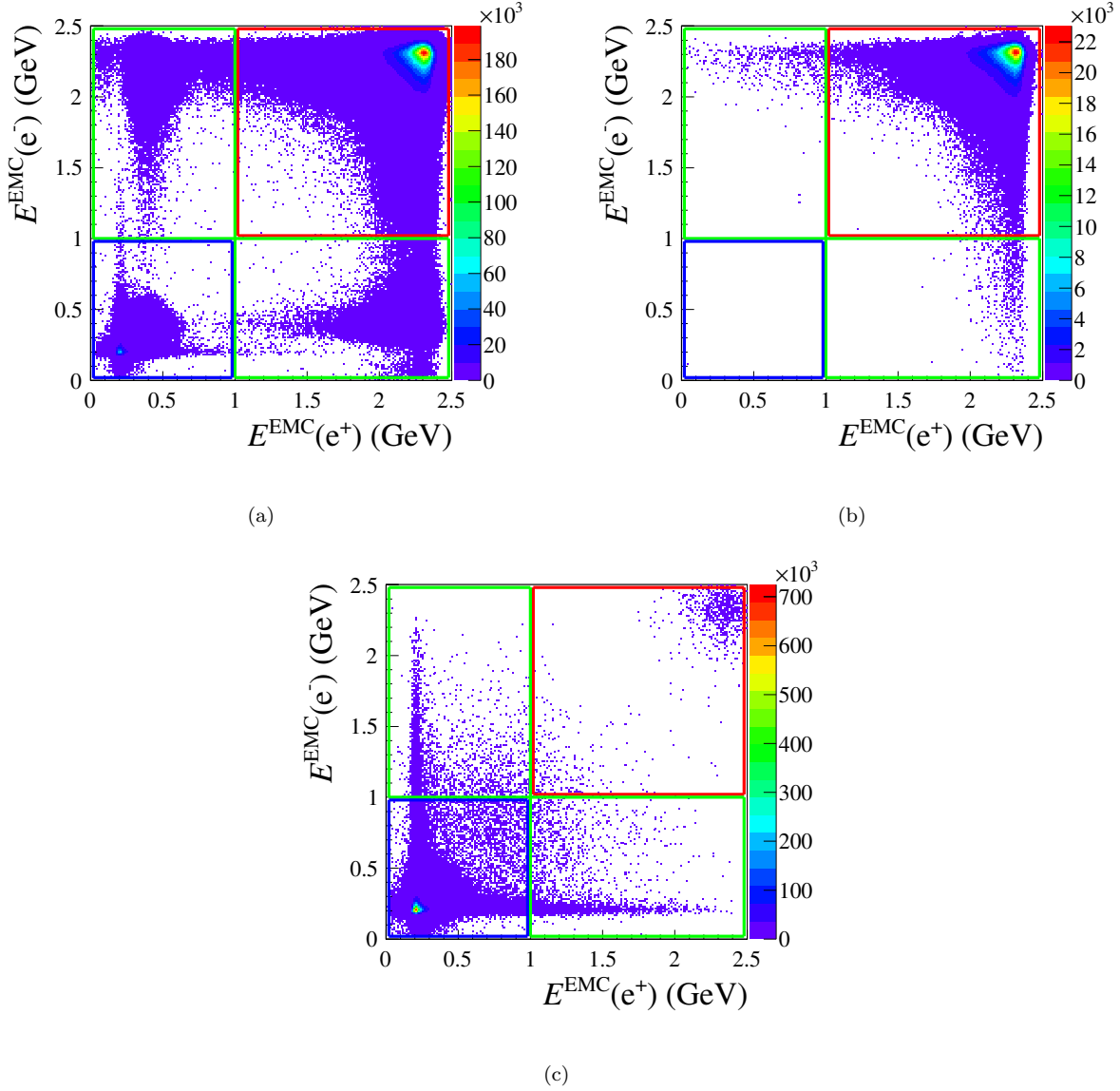


Figure 4. The two-dimensional distributions of $E^{\text{EMC}}(e^-)$ versus $E^{\text{EMC}}(e^+)$ in data (a), Bhabha MC sample (b) and background MC samples (c) for the 4620 MeV energy point. Three kinematic regions are presented: red square region [$E^{\text{EMC}}(e^+) > 1$ GeV and $E^{\text{EMC}}(e^-) > 1$ GeV] for the NORMAL SAMPLE, and the remaining regions for the SATURATION SAMPLE. The dimuon backgrounds concentrate in the blue square [$E^{\text{EMC}}(e^+) < 1$ GeV and $E^{\text{EMC}}(e^-) < 1$ GeV], as shown in plot(c).

evaluate the relative size of this effect, the sample is divided into two categories: NORMAL SAMPLE ($E^{\text{EMC}}(e^+) > 1$ GeV and $E^{\text{EMC}}(e^-) > 1$ GeV) without saturated e^+e^- EMC clusters and SATURATION SAMPLE ($E^{\text{EMC}}(e^+) < 1$ GeV or $E^{\text{EMC}}(e^-) < 1$ GeV) with at least one saturated e^+ or e^- EMC cluster. However, as shown in Fig. 4(b), MC simulations do not reflect the saturation effect. In order to obtain the total signal yields correctly matching the MC-determined efficiency, the signal yields in both the NORMAL SAMPLE and the SATURATION SAMPLE are counted in.

For the NORMAL SAMPLE, backgrounds are negligible compared to the statistics of the signal yields, which is validated by using the background MC sample which contains the inclusive MC sample and all QED events except the Bhabha signal, as shown in Fig. 4(c). Hence, the survived NORMAL SAMPLE is taken as the signal. For the SATURATION SAMPLE, a portion of the background is from the dimuon process $e^+e^- \rightarrow \mu^+\mu^-$, as indicated in Fig. 4(c). To extract the signal yields, the normalized pulse height, PH_{norm} , from the specific ionization energy lost by the charged track in the MDC is adopted to distinguish the Bhabha events from the dimuon backgrounds. Figure 5 shows the fit to the PH_{norm} distribution, where the signals peak around 1.0 for the electron and the dimuon backgrounds peak around 0.86. In the fit, the shape of the electron signals is modelled using the electron sample in the NORMAL SAMPLE, and the muon shape is taken from the control sample of the dimuon process, where the depth of the dimuon tracks penetrating into the muon counter is required to be larger than 10 cm and is implemented for data in the background region ($E^{\text{EMC}}(e^+) < 1$ GeV and $E^{\text{EMC}}(e^-) < 1$ GeV) in Fig. 4(a). The fitted yields of the Bhabha process are taken as signals in the SATURATION SAMPLE.

The sum of the signal yields in the NORMAL SAMPLE and SATURATION SAMPLE is taken as the total yield of the Bhabha events. The detection efficiency is estimated by using the Bhabha MC samples, and the observed Bhabha cross section is calculated based on the BabaYaga@NLO generator. Therefore, the integrated luminosity of the data sample is calculated using Eq. (3) and the corresponding results for the 12 energy points are given in Table 1. The statistical precision of the measured luminosity is better than 0.05% at each energy point.

Sources of systematic uncertainties in the luminosity measurement are summarized in Table 4. For the 12 energy points, common systematic uncertain-

ties are assigned. Details are discussed as follows.

Table 3. Configuration of the BabaYaga@NLO generator used for simulating Bhabha events.

Parameter	Value
E_{cms}	refer to Table 1
Beam energy spread	1.58 MeV
MinThetaAngle	20°
MaxThetaAngle	160°
Maximum Acollinearity	180°
NSearch	4000000
RunningAlpha	1
Number of photon	-1

High momentum electron samples are selected to study the systematic uncertainties due to tracking, the nCharged requirement, the momentum requirement and the $\cos\theta$ requirement. We select one e^+ , with momentum larger than 2 GeV/c and $E^{\text{EMC}}(e^+)$ greater than 1 GeV as the positron candidate from the Bhabha process, and take the recoil e^- as the control sample to study the efficiency of the selection criteria. The relative efficiency difference between the control sample and the Bhabha MC sample is regarded as the systematic uncertainty.

Table 4. Systematic uncertainties on the luminosity measurement. The total systematic uncertainty corresponds to the quadrature sum of each item.

Source	Uncertainty (%)
Tracking efficiency	0.30
nCharged requirement	0.10
Momentum requirement	0.18
$\cos\theta$ requirement	0.30
Saturation events	0.20
BabaYaga@NLO generator	0.10
MC statistics	0.05
Cross section	0.09
Total	0.53

For estimation of the signal yields, the main systematic issue is in the extraction of the signal yields in the SATURATION SAMPLE. As a check, a different method of counting the number of survived events has been adopted after removing the dimuon backgrounds by discarding events in the region $E^{\text{EMC}}(e^+) < 1$ GeV and $E^{\text{EMC}}(e^-) < 1$ GeV. In the remaining events of

the SATURATION SAMPLE, there is a small fraction of backgrounds (about 0.50%), which is neglected. The resultant luminosity differs from the nominal result by 0.20%, which is taken as the systematic uncertainty.

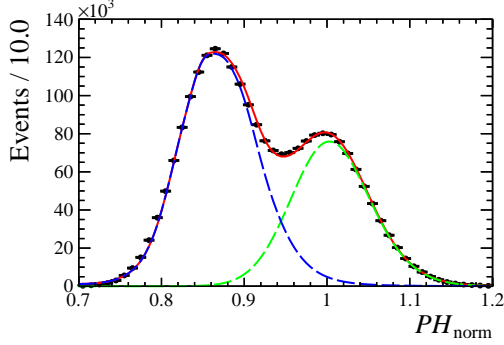


Figure 5. Fit to the PH_{norm} distribution in the SATURATION SAMPLE from the 4620 MeV data sample. Black dots with error bars are data, the red line is the total fit, the long dashed blue line is background dominated by the dimuon process, and the dashed green line represents saturation events.

For the BabaYaga@NLO Generator, the theoretical uncertainty of the cross section calculation is assigned to be 0.10% [31]. The systematic uncertainty caused by MC statistics is estimated to be 0.05% according to the generated 5 million Bhabha MC events for each energy point.

To study the effect due to the E_{cms} uncertainty on the cross section calculation in the BabaYaga@NLO generator, the input values of E_{cms} have been varied within 2 MeV and the corresponding maximum change on the obtained cross section is taken as the systematic uncertainty.

As a cross check, the di-photon process is used to obtain the luminosity. To select the signal candidates, we require that there are at least two shower clusters

in the EMC and no charged tracks detected in the MDC. The clusters must satisfy $|\cos\theta^{\text{EMC}}| < 0.8$. To select back-to-back photon showers and reduce the backgrounds of Bhabha events, their angles with respect to the IP are required to be larger than 178° and $\Delta\phi^{\text{EMC}}$ of the two showers must be within $[-3^\circ, 3^\circ]$. To account for the EMC saturation effect and reduce the dimuon backgrounds, the hit number of one EMC shower is required to be larger than 20. The requirements are optimized based on the inclusive MC sample. The cross section and detection efficiency are determined by the BabaYaga@NLO generator. Using Eq. (3), the resultant luminosity results at different energy points and the ratios between the measured luminosities based on the Bhabha and di-photon processes are consistent with unity, as given in Table 1.

5 Summary

The center-of-mass energies and the integrated luminosities of the e^+e^- annihilation data between 4.61 GeV and 4.95 GeV collected from the years 2020 to 2021 with the BESIII detector at the BEPCII collider have been measured with high precision. By adopting a novel method for analyzing $\Lambda_c^+\bar{\Lambda}_c^-$ pair-production in electron-positron annihilations, the center-of-mass energies are measured with a precision of ~ 0.6 MeV, which is dominated by the precision of the known Λ_c mass. The integrated luminosities of the collected data samples are measured with a precision better than 1% by analyzing large-angle Bhabha scattering events, after taking into account the EMC saturation effect. These results offer fundamental inputs for physics analyses based on these data samples.

The BESIII collaboration thanks the staff of BEPCII and the IHEP computing center for their strong support.

References

- 1 N. Brambilla, S. Eidelman, C. Hanhart, A. Nefediev, C. P. Shen, C. E. Thomas, A. Vairo and C. Z. Yuan, Phys. Rept. **873**, 1-154 (2020).
- 2 F. K. Guo, C. Hanhart, U. G. Meißner, Q. Wang, Q. Zhao and B. S. Zou, Rev. Mod. Phys. **90**, 015004 (2018).
- 3 H. X. Chen, W. Chen, X. Liu and S. L. Zhu, Phys. Rept. **639**, 1-121 (2016).
- 4 S. L. Olsen, T. Skwarnicki and D. Zieminska, Rev. Mod. Phys. **90**, 015003 (2018).
- 5 S. L. Olsen, Front. Phys. (Beijing) **10**, 121-154 (2015).
- 6 N. Brambilla, S. Eidelman, B. K. Heltsley, R. Vogt, G. T. Bodwin, E. Eichten, A. D. Frawley, A. B. Meyer, R. E. Mitchell and V. Papadimitriou, *et al.* Eur. Phys. J. C **71**, 1534 (2011).
- 7 M. Ablikim *et al.* (BESIII Collaboration), Phys. Rev. Lett. **126**, 102001 (2021).
- 8 H. B. Li and X. R. Lyu, Natl. Sci. Rev. **8**, nwab181 (2021).
- 9 M. Ablikim *et al.* [BESIII], Phys. Rev. Lett. **116**, no.5, 052001 (2016).
- 10 M. Ablikim *et al.* [BESIII], Phys. Rev. Lett. **115**, no.22, 221805 (2015).
- 11 M. Ablikim *et al.* [BESIII], Phys. Rev. Lett. **121**, no.6, 062003 (2018).
- 12 M. Ablikim *et al.* [BESIII], Phys. Rev. Lett. **121**, no.25,

- 251801 (2018).
- 13 M. Ablikim *et al.* [BESIII], Phys. Rev. Lett. **120**, no.13, 132001 (2018).
- 14 M. Ablikim *et al.* [BESIII], Phys. Rev. D **103**, no.9, L091101 (2021).
- 15 H. Y. Cheng, [arXiv:2109.01216 [hep-ph]].
- 16 Nucl. Instrum. Meth. A **659** (2011), 21-29
- 17 B.Wang, L.Y. Dong and X.D. Ruan, Nuclear Electronics and Detection Technology, **33**, 240-244(2013). <https://kn.s.cnki.net/kcms/detail/detail.aspx?dbcode=CJFD&dbname=CJFD2013&filename=HERE201302028&uniplatform=NZKPT&v=ZDq7EQ0DJ6choXbFr3DRbj5vsa5ghdG0GsHdrrnW6X0-ka70Krq6Tk2G6ct25vmPC>
- 18 M. Ablikim *et al.* (BESIII Collaboration), Nucl. Instrum. Meth. A **614**, 345-399 (2010).
- 19 C. H. Yu *et al.*, Proceedings of IPAC2016, Busan, Korea, 2016, doi:10.18429/JACoW-IPAC2016-TUYA01.
- 20 M. Ablikim *et al.* (BESIII Collaboration), Chin. Phys. C **44**, 040001 (2020).
- 21 X. Li *et al.*, Radiat. Detect. Technol. Methods **1**, 13 (2017); Y. X. Guo *et al.*, Radiat. Detect. Technol. Methods **1**, 15 (2017); P. Cao *et al.*, Nucl. Instrum. Meth. A **953**, 163053 (2020).
- 22 S. Agostinelli *et al.* (GEANT4 Collaboration), Nucl. Instrum. Meth. A **506**, 250 (2003).
- 23 S. Jadach, B. F. L. Ward and Z. Was, Phys. Rev. D **63**, 113009 (2001); Comput. Phys. Commun. **130**, 260 (2000).
- 24 D. J. Lange, Nucl. Instrum. Meth. A **462**, 152 (2001); R. G. Ping, Chin. Phys. C **32**, 599 (2008).
- 25 P. A. Zyla *et al.* (Particle Data Group), PTEP **2020**, 083C01 (2020).
- 26 B. Aubert *et al.* (BaBar Collaboration), Phys. Rev. D **72**, 052006 (2005)
- 27 J. C. Chen, G. S. Huang, X. R. Qi, D. H. Zhang and Y. S. Zhu, Phys. Rev. D **62**, 034003 (2000); R. L. Yang, R. G. Ping and H. Chen, Chin. Phys. Lett. **31**, 061301 (2014).
- 28 E. Richter-Was, Phys. Lett. B **303**, 163 (1993).
- 29 M. Ablikim *et al.* (BESIII Collaboration), Phys. Rev. Lett. **112**, 132001 (2014).
- 30 A. D. Bukin, Fitting function for asymmetric peaks, arXiv:0711.4449.
- 31 G. Balossini, C. Bignamini, C. M. C. Calame, G. Montagna, O. Nicosini and F. Piccinini, Phys. Lett. B **663**, 209-213 (2008).
- 32 M. Ablikim *et al.* (BESIII Collaboration), [arXiv:2203.03133 [hep-ex]].